Surface science issues in plasma etching

by G. S. Oehrlein
M. F. Doemling
B. E. E. Kastenmeier
P. J. Matsuo
N. R. Rueger
M. Schaepkens
T. E. F. M. Standaert

Pattern transfer by plasma-based etching is one of several key processes required for fabricating silicon-based integrated circuits. We present a brief review of elementary plasma-etching processes on surfaces and within integrated-circuit microstructures—and an overview of recent work in our laboratory on plasma-etching aspects of the formation of self-aligned contacts to a polysilicon layer through a SiO_2 layer and a Si_3N_4 etch-stop layer. The work illustrates the richness of associated surface science issues that must be understood and controlled in order to most effectively achieve plasma-based pattern transfer.

Introduction and motivation

Plasma etching is currently widely used in the fabrication of silicon-based integrated circuits. The process is used to produce high-resolution patterns in many of the thin layers of the circuits and to selectively remove masking layers [1, 2]; it is based on the following sequence of microscopic reaction steps. Electrons are accelerated by rf or microwave electric fields and collide inelastically with suitable precursor molecules to produce ions, atoms, and radicals. A complex mixture of reactive species is produced. Neutral and ionic reactive species strike the surfaces that are in contact with them to form products that are volatile. The consequences of plasma–surface interactions are to a significant extent controlled by the incident ion fluxes and their energies. An electron-free space-charge region designated as a "sheath" forms between a plasma and a contacting solid surface. Sheaths are of critical importance for plasma etching, since positive ions are accelerated toward the surface when entering a sheath. The accelerated ions bombard the surface with energies that are much greater than thermal energies. This results in nonthermal interactions that are in many instances dominant in controlling the outcome of a plasma-etching process. The controlled patterning of thin layers by a plasma-etching process requires a rapid chemical reaction rate of the incident species with the layers, and that the reaction products have a high vapor pressure at the substrate temperature.

A plasma process that is used to transfer lithographically defined patterns into a thin layer must satisfy constraints that include dimensional control, etch selectivity to the mask and the underlying surface or layer, and an acceptable process rate; additionally, the process should not damage devices that may be present on the substrate. One key prerequisite to achieving these goals is the control of plasma–surface interactions. In this paper, we review important plasma–surface-interaction phenomena that are pertinent to the plasma etching of layers of interest in the silicon-based integrated-circuit technology. The first part of the paper is an introduction to relevant scientific issues, and for completeness repeats several discussions presented in a recent review [2].

©Copyright 1999 by International Business Machines Corporation. Copying in printed form for private use is permitted without payment of royalty provided that (1) each reproduction is done without alteration and (2) the *Journal* reference and IBM copyright notice are included on the first page. The title and abstract, but no other portions, of this paper may be copied or distributed royalty free without further permission by computer-based and other information-service systems. Permission to *republish* any other portion of this paper must be obtained from the Editor.

0018-8646/99/$5.00 © 1999 IBM

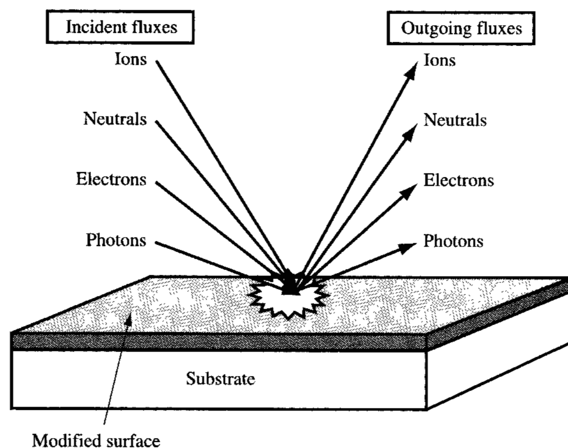

Figure 1

Schematic diagram of incident and outgoing particle fluxes at a surface in contact with a low-pressure etching plasma. The surface processes that occur are detailed in Table 1.

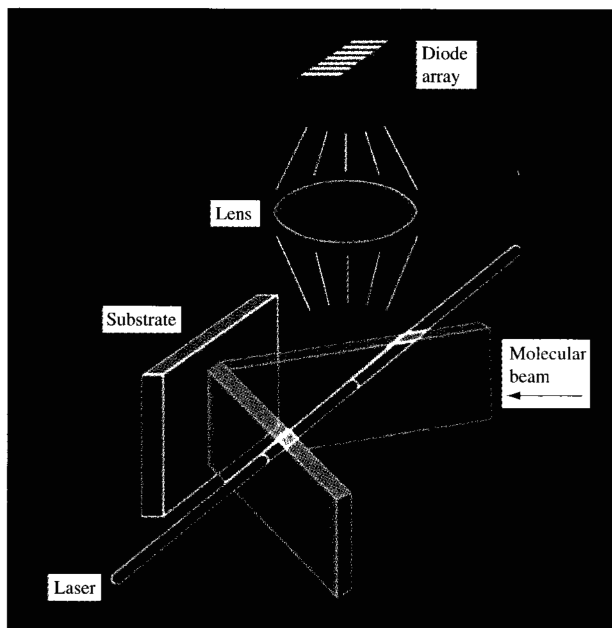

Figure 2

Schematic of the imaging of radicals interacting with a surface (IRIS) technique. From [9], with permission.

Subsequently, an overview is presented of current work in our laboratory on surface science issues pertaining to an important plasma-etching application: the etching of via holes for forming self-aligned contacts to a polysilicon layer. The final section briefly describes related approaches, for which well-characterized beams of reactive species that exist in plasmas are employed to gain more fundamental insights into plasma–surface interactions.

Plasma–surface interactions

- *Planar surfaces*

A surface in contact with a process plasma is exposed to fluxes of neutral atoms, molecules, ions, electrons, and photons, which in turn stimulate the production of outgoing fluxes of neutrals, ions, electrons, and photons. A modified surface layer is produced by these processes, as shown schematically in **Figure 1**. Associated physical and chemical surface processes are listed in **Table 1** [2].

In situations of practical interest, the plasma-etching reaction is dominated by the incident fluxes of ions, neutrals, and electrons, whereas photon bombardment plays a negligible role. The plasmas used for integrated-circuit processing are weakly ionized, with an ion/neutral ratio that can range from less than 10^{-6} to about 0.1 [3]. Although the neutral flux to the surface is dominant, the ability to produce directional (vertical) etching profiles is due to bombardment of the substrate with positive ions. Often the achievement of the process objectives—etching rate, directionality, selectivity—requires the use of multiple species fluxes with differing energies. Certain species fluxes that are incident at the surface may not be desirable or necessary to achieve process objectives, but are unavoidable because of the use of the plasma environment.

Various reactors have evolved that are best suited to satisfy the needs of particular applications, and the absolute values of the surface fluxes and the flux ratios vary significantly between these reactors. High-resolution pattern transfer requires controllable ion bombardment to achieve the profile and selectivity goals of the process of interest and is typically conducted at pressures of less than 100 mTorr. In recent years, a significant effort has been devoted to developing high-density plasma reactors that function at pressures of 10 mTorr or less, where it is easier to produce highly directional etching profiles and control feature-size-dependent etching phenomena [4, 5]. High-density plasma-etching equipment employs two power supplies, making it possible to separately control ion density and ion energy. Ion density is adjusted by the source power level, whereas ion energies are controlled with a separate "bias" power supply [3]. At the opposite end of the spectrum of plasma-etching reactors are high-pressure, remote plasma tools. These are used for highly selective etching (e.g., resist mask stripping) for which etching directionality is not required. Resist mask stripping processes employ gas pressures near ~1 Torr,

Table 1 Surface processes that are important in the plasma processing of thin layers of interest in the silicon-based integrated-circuit technology. From [2], with permission.

Processes	*References*
1. Adsorption rates of radicals at specific surfaces	[25]
2. Reaction rates to form intermediate or stable products	[25]
3. Desorption rates	[25]
4. Effect of simultaneous ion and electron bombardment on adsorption, reaction, and desorption	[25, 55, 63–65]
5. Particle and energy reflection during ion bombardment	[66]
6. Ion implantation and production of defects	[67]
7. Sputtering	[42–44, 64]
8. Diffusion effects (on the surface, through the reaction layer, ion-enhanced diffusion effects, etc.)	[64, 67]
9. Desorbed product redeposition phenomena (on the sidewalls of structures, walls of the reactor, etc.)	[19]
10. Surface roughening (intrinsic, micromasking)	[68]
11. Electron emission	[3, 62]
12. Photostimulated processes	[69, 70]
13. Metastable induced processes	[71]

and wafers are located downstream from the plasma, thus preventing exposure to charged species and photons.

Establishing and quantitatively describing a surface reaction mechanism in the plasma environment requires, first, characterization of the incident species fluxes, e.g., as a function of composition, energy, angle, and so forth; second, determination of the surface processes, e.g., adsorption, reflection, direct reaction behavior of the incident species, measurement of the surface coverage, characterization of the processes in the reaction layer, and so forth; and third, determination of the reaction products (their chemical identity, energy content, product desorption mechanism, etc.). Ideally we would like to characterize and quantify the importance of each of the elementary surface processes listed in Table 1 for the important plasma and surface species, and relate these to measured etching or deposition rates, film properties, etc.

Techniques for incident and outgoing flux analysis of a broad set of species Often based on optical techniques [2, 6] or mass spectrometry [7, 8], these techniques provide an overview of a broad set of species. Significant adaptation of these techniques to address issues connected with the plasma process environment has occurred in recent years. One development is illustrative of these efforts: the imaging of radicals interacting with a surface (IRIS) technique. The technique provides important information on the interaction of specific radicals with a realistic surface; it is schematically depicted in **Figure 2** [9]. A plasma chamber is in contact with a high-vacuum chamber containing the substrate. A molecular beam is produced, strikes the surface, and is partly reflected. Light from a dye laser optically excites specific radicals in the incident and reflected beams. The light emission from these radicals is then measured and used to extract information on their density. The measurement can be performed with and without a surface present. By taking the difference of the emission data, it is possible to determine the intensity of scattered radicals and the reactivity of specific radicals with particular surfaces.

Techniques for surface characterization In most cases, such techniques cannot be used in real time for the characterization of plasma–surface interactions because of the high pressure and corrosive plasma process environment. However, many of the plasma-modified surfaces are stable in ultrahigh vacuum (UHV). Significant insights regarding the mechanisms that limit etching reactions can be obtained from studies of the stable plasma-modified surface in UHV as a function of process conditions, and by comparing the data obtained with changes in surface-etching behavior. The use of optical real-time measurement techniques (for example, ellipsometry [10], and Fourier transform infrared spectroscopy [11, 12]) enables researchers to test assumptions regarding the stability of the plasma-modified surfaces. A listing of these techniques has been provided in Reference [2].

We conclude that, for planar surfaces, an impressive array of techniques exist that can be used to probe various aspects of plasma–surface interactions in order to identify relevant physical and chemical mechanisms.

• *Microstructures*

The most important use of plasma-etching processes is in the production of the microscopic features of integrated circuits. When exposing three-dimensional patterned structures to a plasma, many novel phenomena take place inside the microstructures that are absent for blanket films. These microstructure-related processes often determine the technological usefulness of the plasma process. The geometry and dimensions of the

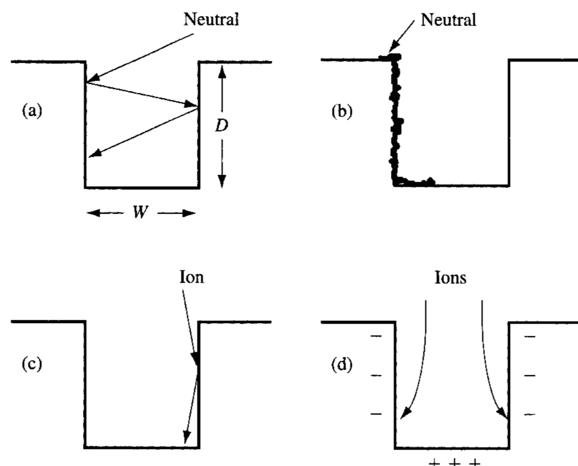

Figure 3

Relevant processes in microstructures: (a) neutral scattering on the sidewalls; (b) neutral diffusion along a sidewall; (c) ion scattering off a sidewall; (d) ion deflection due to differential charging of the sidewalls of insulating layers.

microstructure and the electrical nature of the microstructure sidewalls (insulating or conductive) are key parameters in determining processes in the microstructure. For microstructures of interest to the semiconductor community, the microstructure widths W and depths D are in the range of about 0.1 μm to 10 μm. The gas mean free paths at low pressure are of the order of millimeters. Consequently, molecular transport in the microstructure is not determined by gas-phase collisions of the particles, but by multiple reflections with the walls of the microstructure, and possibly surface diffusion [see **Figures 3(a)** and **3(b)**]. To describe these phenomena in microstructures, we need to know the reflection coefficient and geometry of reflection of neutrals from sidewalls as a function of the plasma parameters and microscopic discharge parameters. Ions also collide with the sidewalls, leading to scattering and energy loss [**Figure 3(c)**]. We would like to know the ion energy loss and the neutralization probability as a function of the angle of incidence of the ions, their energy, and their chemical nature. Differential charging of sidewalls by electrons [**Figure 3(c)**] has also been shown to be important [13, 14]. The magnitude of this effect should vary significantly with the surface conductivity of the thin layers in the plasma environment, which is in most cases not known.

Ideally we would like to have for microstructures the same information listed above for planar surfaces as a function of microstructure geometry. The connection to the technological figures of merit also has to be established. It is therefore imperative to attempt to characterize the effects of the incident and desorbing species fluxes and the surface processes at distinct features of relevant three-dimensional microstructures, e.g., trenches and vias. An attempt to determine experimentally the changes in ion flux when passing through holes in quartz as a function of the aspect ratio of the holes has been reported by Kurihara and Sekine [15]. A fluorocarbon plasma was characterized by mass spectrometry through 100- and 200-μm-thick capillary plates made of lead glass placed on the sampling orifice of the mass spectrometer. The diameter of the holes in the capillary plates ranged from 25 μm to 10 μm, covering aspect ratios from 4 to 20. A reduction of the ion current by more than an order of magnitude relative to planar surfaces was observed. The reduction was less for conditions where the holes in the glass had been coated with a Cu film. These results are helpful in explaining the observed etching behavior of SiO_2 as a function of feature aspect ratio [16, 17].

X-ray photoelectron spectroscopy (XPS) of etched microstructures after vacuum transfer has been used to obtain information on the surface chemistry in three-dimensional patterned structures for a variety of plasma-etching situations [18–24]. This information is also critical to obtaining an understanding of the interaction between different surfaces during plasma etching (e.g., the plasma–surface interaction with a resist mask) and how the reaction products from this interaction change the surface chemistry of etching on a different material (e.g., redeposition of resist etching products on a polycrystalline silicon surface [20]).

- *Role of modified surface layers in achieving plasma process objectives*

The formation of distinct reaction layers at the various surfaces of a microstructure exposed to a process plasma is often intimately linked to achieving the goals of the pattern-transfer process. **Figure 4** shows ideal pattern-transfer characteristics of a plasma-etching process. The indicated characteristics can be approximately achieved if relatively thick ($\geq$2 nm) involatile reaction layers form on critical surfaces during exposure to the plasma. This requires the use of appropriate etching parameters such as the nature and mixture of the feed gases ("etch chemistry"), the plasma density, and the ion energies to nearly balance layer etching and growth. The most important reasons for differences in plasma–surface interactions between distinct surfaces are 1) the ion and energy flux difference at horizontal and vertical surfaces and 2) compositional differences between two distinct materials, e.g., SiO_2 vs. silicon or resist. The plasma–surface interaction changes resulting from these differences often produce thin steady-state passivation

layers (see the finished structure in Figure 4), but can in the extreme case produce a change from net etching to net deposition.

Etching directionality To control the directionality of the etching process, we select process conditions for which the spontaneous etching rates are slow and ion bombardment initiates the etching. In addition, control of lateral etching for reactive layers requires the formation of passivation layers on the vertical walls of the layers. This mechanism is important for patterning of thin films of silicon and aluminum using either resist or SiO_2 masks in fluorine-, chlorine-, and bromine-based plasmas. The composition of the sidewall passivation layers has been studied for various systems [18, 19, 21–23], and the reader is referred to that literature for details.

Etching selectivity This can be achieved by the formation of passivation layers on the horizontal mask and underlayer surfaces. This mechanism is important for SiO_2 etching and is discussed in more detail below.

Plasma etching of integrated-circuit-related layers has been well characterized because of the importance of the integrated-circuit technology. A detailed review of halogen-based plasma-etching chemistries is not within the scope of this paper. For reviews dealing with the surface chemistry of plasma etching of silicon, SiO_2, and Si_3N_4 in various halogens, the reader is referred to two reviews and the references provided there [2, 25]. In the following section we focus on a specific example of a plasma-etching challenge in the current silicon-based integrated-circuit technology. The example chosen is the formation of self-aligned contacts through SiO_2 to a Si_3N_4 etch-stop layer [26]. This particular application is useful in highlighting the richness of the surface chemistry phenomena that must be understood in order to control the plasma-etching aspects of microstructure fabrication. The phenomena discussed are representative of similar issues that must be addressed in other plasma-etching steps during integrated-circuit fabrication.

- *An example: Plasma-etching aspects of the formation of self-aligned contacts to a polysilicon layer*

Figure 5 shows a scanning electron micrograph of the cross section of a self-aligned contact structure. The goal of the associated plasma etching is to initially etch the SiO_2 layer to the Si_3N_4 etch-stop layer that covers the polysilicon (poly-Si) layer [26]. Subsequently, oxide etching should continue in the region next to the poly-Si where the SiO_2 layer is thicker, until the underlying Si_3N_4 layer is encountered. After the SiO_2 etching, the resist mask and the Si_3N_4 etch-stop layer must be removed with high selectivity. Important requirements here are satisfactory SiO_2/Si_3N_4 etching selectivity for different inclinations of

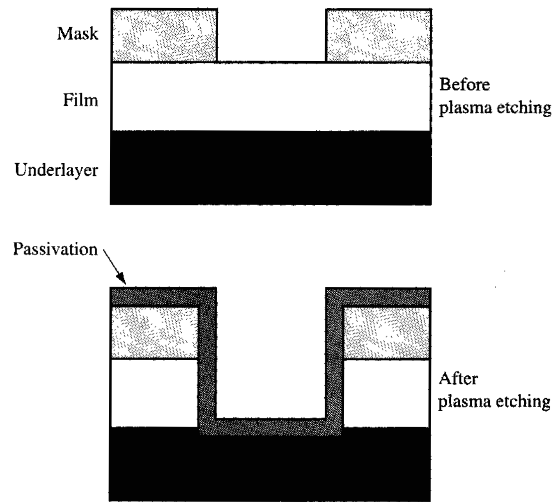

Figure 4

Schematic diagram showing how near-ideal characteristics of pattern transfer by a plasma-etching process are possible by the formation of passivation layers on horizontal and vertical surfaces. The thicknesses of the reaction layers resistant to etching that exist on the horizontal and vertical surfaces are exaggerated in the drawing.

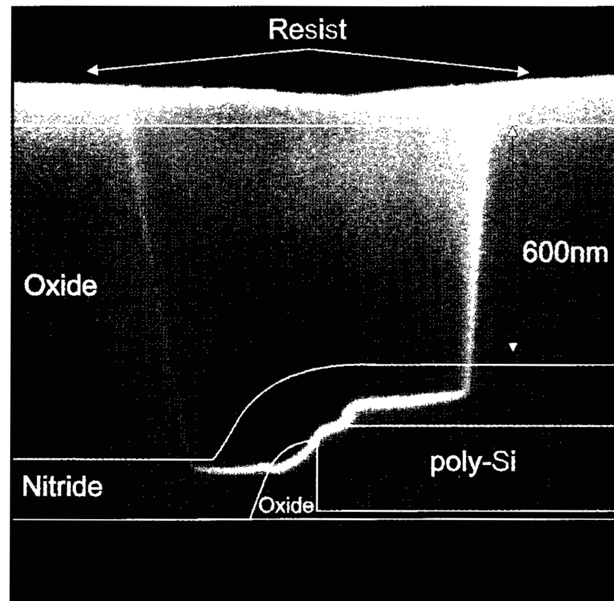

Figure 5

Scanning electron micrograph of the cross section of a self-aligned contact structure, etched under conditions at which only a marginal oxide-to-nitride selectivity could be maintained at the curved nitride etch-stop layer. From [27], with permission.

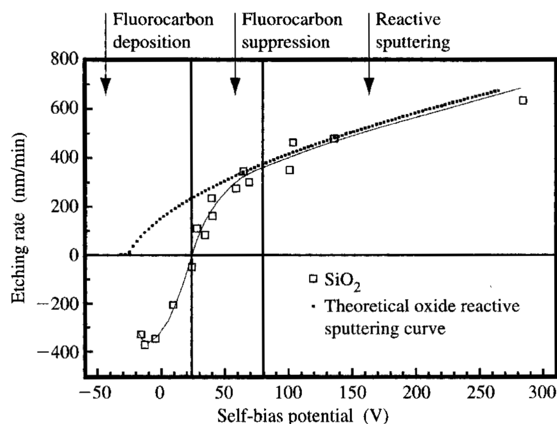

Figure 6

Etching rate of SiO_2 as a function of self-bias potential in a fluorocarbon high-density plasma. Use was made of a CHF_3 plasma and an inductive power level of 1 kW. For comparison, a theoretical oxide-reactive sputtering curve is shown. At high self-bias voltages, the curve fits the etching-rate data and increases as the square root of the ion energy. From [28], with permission.

the Si_3N_4 surface, high SiO_2/resist mask etching selectivity, a near-vertical SiO_2 sidewall angle, and the ability to remove the sacrificial layers (resist and Si_3N_4) with high selectivity relative to SiO_2 and silicon. Finally, a clean silicon contact surface must be formed to control contact resistance of the subsequently formed contact. The structure shown in Figure 5 was produced in conditions under which only a marginal oxide-to-nitride selectivity was achieved at the curved nitride etch-stop layer [27], leading to unacceptable Si_3N_4 loss. The various surface chemical aspects of this process sequence are described below. All of the steps described, except for the isotropic removal of the Si_3N_4 layer, were performed using an inductively coupled high-density plasma etching reactor at low pressures with independent substrate biasing [28]. The Si_3N_4 removal was conducted in a microwave-based plasma-etching system with the wafer located downstream from the plasma [29, 30]. The reader should consult the cited publications for experimental details and further information.

SiO_2 etching and SiO_2 etching selectivity to silicon and Si_3N_4
Fluorine-based plasmas are normally used to pattern SiO_2, since the reaction rates of SiO_2 with the other halogens are small [31]. Because of the chemical inertness of SiO_2, significant ion energies are required to etch SiO_2 layers at an acceptable rate [31–33]. For high ion energies, physical sputtering is an important erosion mechanism, and it becomes difficult to stop etching on a chemically different material (e.g., the underlayer or the mask). Achieving adequate etching selectivity of SiO_2 with respect to the mask and the underlayer is one of the principal difficulties in the patterning of SiO_2 layers using plasma-based methods. The only practical solution to this problem has been an approach in which, during plasma etching, the resist surface and the underlayer (silicon, Si_3N_4, etc.) are covered by a thin steady-state passivation layer to prevent ion-induced etching. This is achieved using fluorine-deficient polymerizing fluorocarbon plasmas [34, 35], e.g., discharges based on CHF_3, CF_4, C_2F_6, C_3F_6, or C_4F_8, with H_2 and CO as possible additives. If a high enough rf bias is applied to the wafer, a complex balance among fluorocarbon deposition, fluorocarbon etching, and substrate etching produces a thin fluorocarbon film on the substrate surface during steady-state etching. The chemical differences between the substrate materials allow for a window of selective etching, since the balance for one material can favor etching while for the other material it can tend toward deposition.

An example of the SiO_2 etching rate as a function of rf bias voltage in a fluorocarbon high-density plasma is shown in **Figure 6**. Without substrate bias, fluorocarbon film formation takes place at a high rate. This fluorocarbon film formation can be suppressed if the substrate is biased above an energy threshold that depends on the discharge chemistry. The atomic oxygen that is produced on the SiO_2 surface by ion bombardment oxidizes the fluorocarbon film precursors (e.g., CF_2) and reduces film formation on the SiO_2 surface. As a result of the competitive process between fluorocarbon deposition and etching, the etch rate of the substrate is controlled by a fluorocarbon film, especially at lower ion energies. Figure 6 shows that the SiO_2 etching curve exhibits several distinct regimes as a function of rf bias voltage; they have been denoted as the *fluorocarbon deposition* regime at low rf bias voltage, the *fluorocarbon suppression* regime for intermediate rf bias conditions, and the *oxide sputtering* regime at high rf bias. The same three regimes are seen in all high-density plasma devices.

Significant differences in fluorocarbon layer thickness on SiO_2 and Si_3N_4 during steady-state etching are indicated by the carbon 1s photoemission spectra plotted in **Figure 7** for a selective SiO_2-to-Si_3N_4 etching process. The photoemission intensity obtained from the etched silicon nitride sample is higher than that from the silicon dioxide sample, indicating that the fluorocarbon film on the nitride surface is thicker than on the oxide surface [36].

In **Figure 8** the etching rates of oxide and silicon nitride at a self-bias potential of −100 V are plotted as a function of fluorocarbon film thickness and are compared to silicon etching under the same conditions. Figure 8 shows that the thickness of the fluorocarbon film depends on the plasma conditions, and the substrate material. The varying

parameter in this plot is the feed-gas composition, which is changed from CHF_3, C_2F_6, C_3F_6 to C_3F_6/H_2. The etching rate of the substrate is inversely proportional to the thickness of the fluorocarbon film, since the film prevents etchants from reaching the substrate.

Important problems in plasma etching of SiO_2 arise from the fact that the selectivity mechanism outlined above presents only an imperfect solution, but the etch-suppressing fluorocarbon film forms to some extent on all surfaces (Figure 8). Silicon dioxide is covered for all conditions by a fairly thin fluorocarbon film (≤2 nm). For the thinnest films, the mechanism of etching can be identified as reactive ion sputtering. The thin fluorocarbon film can be explained by the ability of silicon dioxide to react with the fluorocarbon film, for example through CO_2 formation [37]. It has been found that for fluorocarbon gases such as CF_4 and CHF_3 for which the polymerization rate is low, oxide etching is primarily dependent on the ion flux [28, 38].

For the same conditions, silicon is covered by relatively thick fluorocarbon films that vary in thickness from 2 to 8 nm as process parameters are changed. A discussion of the etching through such films can be found in Reference [38] and is summarized here. Ion penetration is limited to 1–2 nm for 150-eV ions [39]. As the fluorocarbon film thickness increases, the ion species and energy flux that reach the Si substrate decrease. More detailed studies have shown that the silicon etching yield (number of Si atoms removed per ion) rather than the silicon etching rate correlates in a unique fashion with the fluorocarbon film thickness, decreasing exponentially with fluorocarbon film thickness. A possible interpretation of these data that is consistent with the simulations on stopping of fluorocarbon ions in the fluorocarbon film is that the ion energy deposition into the first 1–2 nm of the steady-state fluorocarbon layer rather than into the Si substrate is a major factor in the reduction of the Si etch rate. As the fluorocarbon film grows to a thickness that exceeds 1 nm, the lack of direct ion bombardment and energy deposition onto the Si substrate reduces the importance of ion-assisted etching, and ultimately Si etching occurs only by direct spontaneous reaction with fluorine atoms that have migrated through the fluorocarbon film. Neutral transport through fluorocarbon films of a thickness exceeding about 1 nm dominates the etching process.

The relatively thick fluorocarbon film on silicon can be explained by the fact that fluorine from the gas phase is consumed by the etching of the fluorocarbon film and the silicon substrate. The reaction of fluorine with the fluorocarbon film leads to formation of desorbing fluorocarbon film particles and balances fluorocarbon film deposition, resulting in a steady state. Additionally, ion sputtering at the surface contributes to the desorption of fluorocarbon film particles. The film thickness adjusts itself

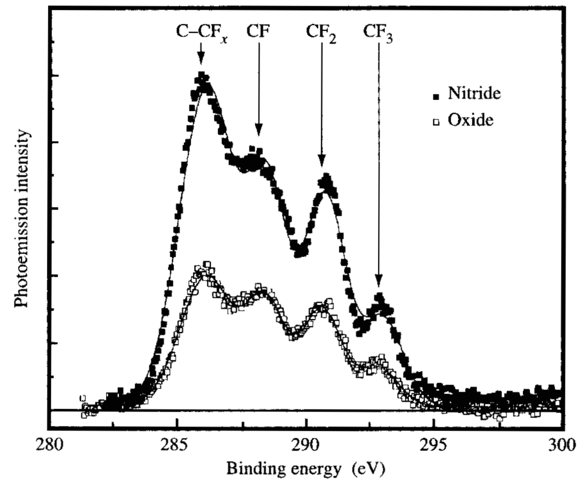

Figure 7

Carbon 1s X-ray photoemission spectra obtained with SiO_2 and Si_3N_4 surfaces etched in a C_3F_6/H_6 plasma at an inductive power of 1400 W, an operating pressure of 6.5 mTorr, and a self-bias of −100 V. The differences in the surface carbon intensity are related to the achievement of SiO_2/Si_3N_4 etching selectivity. From [27], with permission.

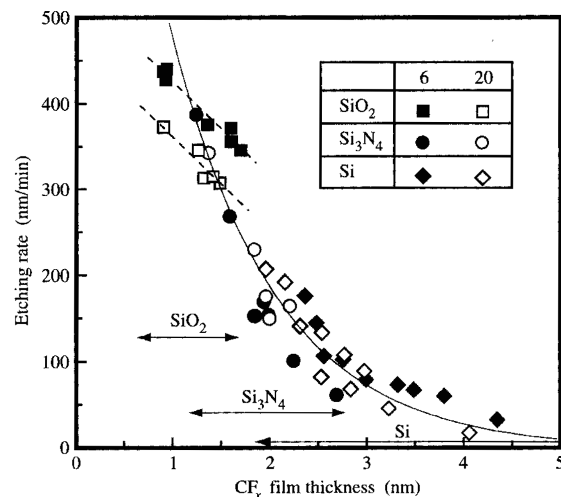

Figure 8

Etching rate vs. fluorocarbon film thickness for SiO_2, Si_3N_4, and silicon. Etching rates and film thicknesses were determined by ellipsometry and XPS for various mixing ratios of C_2F_6/C_3F_6 and at 6 and 20 mTorr. The source power and self-bias potential were fixed at 1400 W and −100 V, respectively. From [36], with permission.

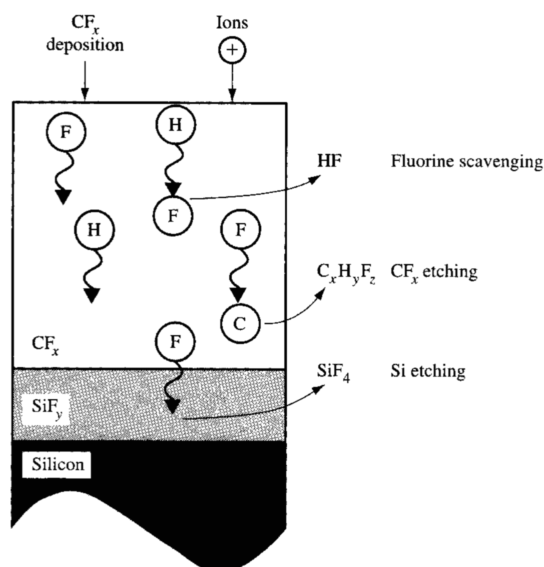

Figure 9

Schematic of the etching dynamics in a thick fluorocarbon film on a silicon substrate. From [38], with permission.

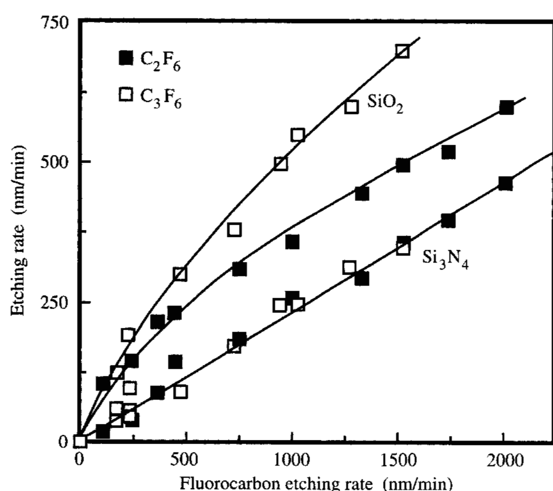

Figure 10

Si_3N_4 and SiO_2 etching rates vs. that of a thick fluorocarbon layer (1400 W source power, 6 mTorr). The varying parameter is the self-bias voltage. The linear relationship for the Si_3N_4 vs. the fluorocarbon layer etching rates indicates that the Si_3N_4 etching rate is controlled by the steady-state fluorocarbon overlayer. This is not the case for the SiO_2.

so that the fluorocarbon film deposition is balanced by the fluorine reaction in the film. The part of the fluorine flux through the fluorocarbon film that is not used for the desorption of fluorocarbon film material reacts with the silicon substrate and forms volatile SiF_4. This process is schematically depicted in **Figure 9**. It is suggested that neutrals are transported through the fluorocarbon film by means of diffusion [40].

For silicon nitride, the etching rates and the steady-state fluorocarbon film thickness lie between those of silicon dioxide and silicon (Figure 8). The experimental data suggest that silicon nitride etching is more like that of silicon than silicon dioxide. An important indication is that the etching rate of the nitride is linearly proportional to that of a fluorocarbon layer (see **Figure 10**). The same relationship has been observed between silicon and fluorocarbon material and is consistent with the fluorine-driven etching process described above [38]. Furthermore, the silicon dioxide data in Figure 10 do not line up with the solid curve as the dashed lines of Figure 8 suggest. This can be explained by the fact that the silicon dioxide etching rate is more dependent on direct ion impact. Hence, the silicon dioxide etching rate has not been found to be proportional to the fluorocarbon etching rate (see Figure 10). For nonselective conditions, Si_3N_4 etches through a mechanism similar to that of SiO_2, i.e., a chemical sputtering mechanism [28].

In the fabrication of self-aligned contact (SAC) structures, the silicon dioxide etching process should terminate on a curved silicon nitride etch-stop layer. In the etching of SAC structures, a reduced oxide-to-nitride selectivity is commonly observed at the corners of the curved nitride etch-stop layer (see Figure 5). To examine the etching behavior and surface chemistry as a function of angle in a controlled fashion, V-groove structures were prepared by highly anisotropic wet etching of silicon substrates [41]. These were covered with either a 380-nm-thick layer of thermally grown oxide or a 100-nm-thick thermal oxide/200-nm-thick silicon nitride stack. The angle between a normal of the V-groove sample surface and that of the average wafer surface was 54.70°. The ion bombardment remained normal to the macroscopic wafer surface, since the V-groove dimensions were at least an order of magnitude smaller than the plasma sheath.

Comparisons of behavior for the planar and the 54.7° inclined surfaces allowed us to identify the most important effects that give rise to SiO_2/Si_3N_4 selectivity loss [27]. The reason for the selectivity loss is not an increase of the Si_3N_4 erosion rate with angle, e.g., as commonly seen in physical sputtering [42–44], but a change in the balance between fluorocarbon film deposition and etching, producing a thinner steady-state fluorocarbon film. The thinner steady-state fluorocarbon film results from an enhanced fluorocarbon etching rate at the curved surface

relative to a planar surface, in conjunction with a lower fluorocarbon deposition rate on the sloped surface (**Figure 11**). The thinner steady-state fluorocarbon passivation layers on the inclined Si_3N_4 surface relative to the flat surface lead to a significantly higher Si_3N_4 etching rate on the angled surfaces relative to the flat surfaces [in this work we found an etching yield ratio between 54.7° and 0° of 2.8 (Figure 11)]. For SiO_2, the etching yield ratio between 54.7° and 0° was found to be 1.33. The oxide-to-nitride etching selectivity was thus reduced at the corners of the curved nitride surfaces. For nonselective SiO_2/Si_3N_4 etching processes (e.g., employing CHF_3), the Si_3N_4 etching rate is not controlled by a steady-state reaction layer, and the enhancement of the Si_3N_4 etching rate shows a different dependence on the angle of incidence. For nonselective Si_3N_4 etching processes, the etching yield ratio difference is 1.4, i.e., similar to that for SiO_2.

For highly polymerizing fluorocarbon gas mixtures and low ion bombardment energies, steady-state fluorocarbon films can also be formed on a SiO_2 surface and can reduce the SiO_2 etching rate [45, 46]. This has important consequences in the etching of high-aspect-ratio features, for which the energy flux to the bottom of the etching feature decreases with increasing aspect ratio (feature depth/width). This ion-flux reduction can be explained by ion deflection caused by electrostatic charging of the SiO_2 sidewalls [13, 15] and/or charging of the resist mask [47, 48]. As the energy flux to the SiO_2 surface decreases with aspect ratio, a thin fluorocarbon film starts to grow on the SiO_2 and reduces the etching rate further, ultimately resulting in fluorocarbon deposition. This etching-deposition transition model can explain the strong slowdown of SiO_2 etching rates at low pressures in high-aspect-ratio features if highly polymerizing gas mixtures are used [16, 17].

Controlling factors in resist erosion Excessive resist loss during fluorocarbon-based high-density plasma etching of SiO_2 features is of significant concern in the integrated-circuit technology. The mechanisms of resist erosion are poorly understood, but recent studies performed using CHF_3, C_3F_6, and C_3F_6/H_2 plasmas have provided important insights regarding the factors that limit such erosion. The reader is referred for details to the work of Doemling et al. [49].

Figure 12 shows the photoresist erosion rates measured in a CHF_3 plasma at 6 mTorr for inductive powers and at 400, 600, and 1400 W as a function of the self-bias potential. The curves are qualitatively similar to the one shown above for SiO_2. A striking result was that as the power was increased from 600 W to 1400 W, no change in the resist etching rate was seen for a given bias voltage. This result implies that the increase of the ion current at the wafer from 6.5 mA/cm^2 at 600 W to 17 mA/cm^2 at

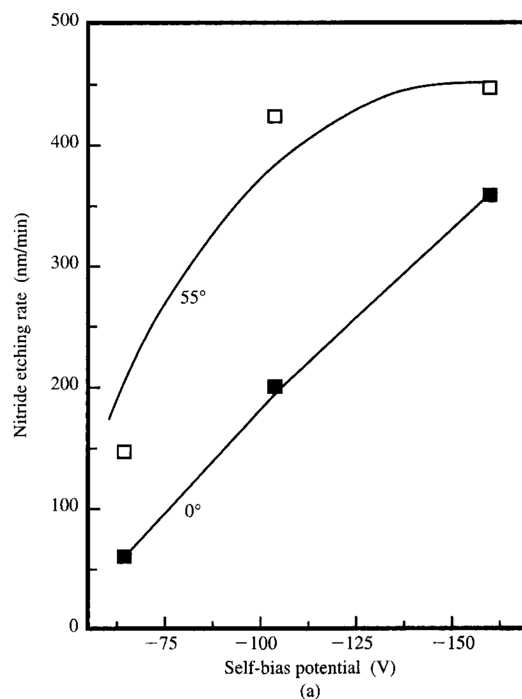

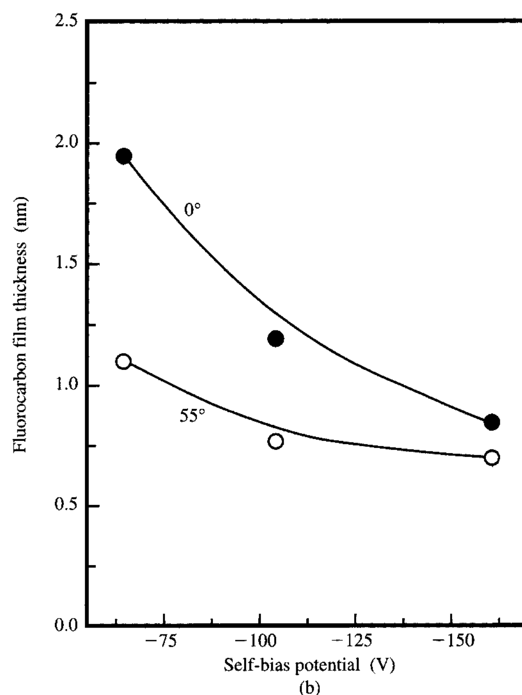

Figure 11

(a) Nitride etching rates and (b) corresponding fluorocarbon film thicknesses as a function of self-bias voltage in a C_3F_6 plasma at 1400 W and 6.5 mTorr on both flat (0°) and angled (55°) surfaces. The data for the angled surfaces were obtained with silicon V-groove samples overcoated with a Si_3N_4 film. From [27], with permission.

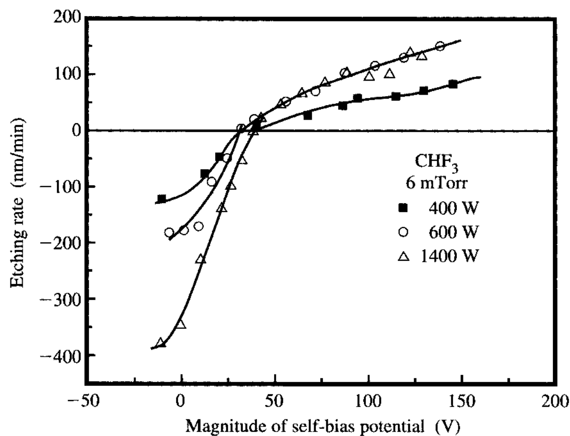

Figure 12

Resist etching rates vs. self-bias potential for different inductive power levels. Note that the resist etching rates are the same at 600 W and 1400 W, and depend only on the self-bias potential (ion energy). From [49], with permission.

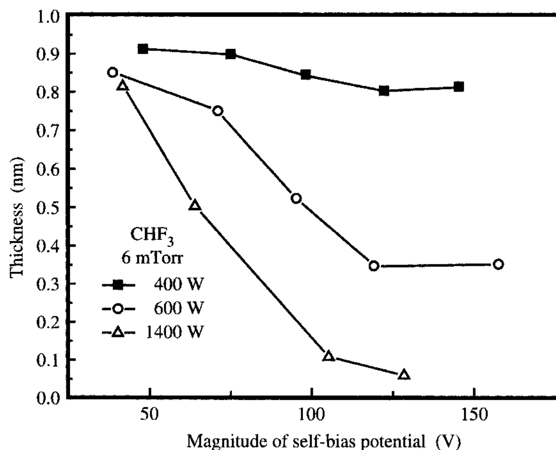

Figure 13

Fluorocarbon film thickness vs. self-bias potential for samples used to obtain the data of Figure 12. From [49], with permission.

1400 W is unimportant for resist etching, a behavior that is dramatically different from that of SiO_2, for which the etching rate increases linearly with ion current. Similar observations were made when using CHF_3 discharges operated at different pressures, or employing C_3F_6/H_2 discharges. The relative trends in F density were determined by fluorine optical emission actinometry. For hydrogen-containing discharges, the F/Ar ratio changed by less than 30% as the inductive power was varied over the entire range, whereas for fluorocarbon discharges without hydrogen present, the F/Ar ratio changed by more than an order of magnitude. This is explained by the strong interaction of hydrogen with fluorine to form HF, which prevents the increase of the fluorine atom concentration in hydrogen-containing fluorocarbon discharges as the source power is increased [31].

To determine whether resist etching is controlled by a steady-state fluorocarbon-layer formation mechanism similar to that for silicon and Si_3N_4 surfaces, fluorocarbon film thicknesses on resist were examined for the samples of Figure 12. **Figure 13** shows the fluorocarbon film thicknesses obtained. For a small self-bias potential (low ion energies), similar fluorocarbon film thicknesses were obtained for all three conditions. With increasing self-bias voltage, a strong reduction of the fluorocarbon film thickness was found at inductive power levels of 600 W and 1400 W. At 400 W, there was only a slight change in fluorocarbon film thickness with increasing self-bias potential. At low inductive power, the ion current is apparently too small to enable the thinning of the fluorocarbon film, and the steady-state fluorocarbon film thickness remains high even at a large self-bias potential.

For fluorine-deficient fluorocarbon discharges that contain hydrogen, the following resist-erosion model is suggested by the above data.[1] At a low rf bias power level, a fairly thick fluorocarbon film covers the resist. The resist etching rate is total-energy-limited and depends on the ion current. As the rf bias power is increased, and provided that the ion current is high enough, a transition from a total rf-bias-power-limited (energy flux) to an rf-bias-voltage-limited (maximum ion energy) behavior is observed. For fluorine-deficient plasmas, this is mirrored in a transition from a thick to a thin steady-state fluorocarbon film, and an increase of the resist etching rate. For high inductive powers the fluorocarbon film thickness is thin enough that the resist erosion rate is no longer limited by the fluorocarbon film. For these conditions the etching rate no longer shows an ion flux dependence, but increases with ion energy. The dependence on ion energy is presumably related to the extent of the modification of the layer in which reaction products are formed, e.g., by the interaction with fluorine atoms.

Cleaning of contact- and via-hole surfaces To minimize the contact resistance between the silicon and the first level of metallization, it is important to produce a clean silicon surface following contact-hole etching. In the

[1] For fluorocarbon discharges without hydrogen, e.g., containing only C_3F_6, for which the fluorine-atom concentration is much higher, the behavior is significantly different, but the use of such discharges for selective etching is limited.

absence of a sacrificial Si_3N_4 layer, the contamination would be a fluorocarbon film (In contact-hole etching with a Si_3N_4 etch-stop layer, this layer must be removed first, as discussed below.). In contact-hole etching, in which the SiO_2 is etched down to a silicon or metal surface, the simplest approach is to perform *in situ* resist stripping in a high-density etching reactor and concurrently remove the fluorocarbon residue from the silicon/metal surface. The cleaning efficiency of this approach can be studied as follows. Beginning with a clean silicon surface, the sample is exposed to a CHF_3 plasma. With the bias applied to the sample, this simulates the over-etching environment during the dielectric etching step and leaves a fluorocarbon residue on the sample surface. Subsequently, an O_2 plasma is used to remove the fluorocarbon film and the resist mask. The O_2 plasma oxidizes the silicon surface. In the final step, the oxide is removed using an Ar discharge with a self-bias potential at the wafer (Ar^+ sputtering).

Figure 14 shows the thickness of the modified layer on the silicon surface, as determined by real-time ellipsometry, during the above processing sequence. The clean surface was exposed to the fluorocarbon plasma environment at time (a), forming a thick fluorocarbon layer. At (b), an rf bias voltage was applied to the sample, and the film was quickly removed. The sample was exposed for 15 s upon complete removal of the fluorocarbon film to simulate over-etching. This allowed a steady-state fluorocarbon layer to be formed. To remove the fluorocarbon layer, e.g., as a result of O_2 resist mask stripping during an actual process sequence, the sample was exposed to an O_2 plasma at (c). The O_2 exposure removed the fluorocarbon layer, and a thick oxide layer began to grow. At (d), the oxidized layer was removed by Ar^+ sputtering and the silicon surface returned to its original state.

Each stage in this process was evaluated using XPS, and the results are shown in **Figure 15**. Part (a) represents the state of the Si after an HF dip, part (b) after the fluorocarbon plasma exposure, part (c) after the O_2 plasma exposure, and part (d) after Ar^+ sputtering. The peaks located at a higher bonding energy than the elemental silicon 2p peak in (b) have been attributed respectively to silicon-bonded 1, 2, 3, and 4 fluorine atoms [10]. As expected, there was a significant amount of reacted Si present after the dielectric etching step. The varying overall intensities were due to the presence of an overlayer, e.g., in part (b), a thick fluorocarbon film.

With the evolution of feature sizes to submicron dimensions, *RC* delay becomes a critical factor in the overall performance of logic chips containing multilevel interconnections. There are two conventional ways of reducing the *RC* delay, one of which is to use interconnect metals with lower resistivity, the other being the use of dielectrics with a lower dielectric constant (low *K*). Recent advances using copper have motivated our study of the removal of the post-dielectric etch fluorocarbon residue using an O_2 plasma-cleaning step followed by Ar^+ sputtering.

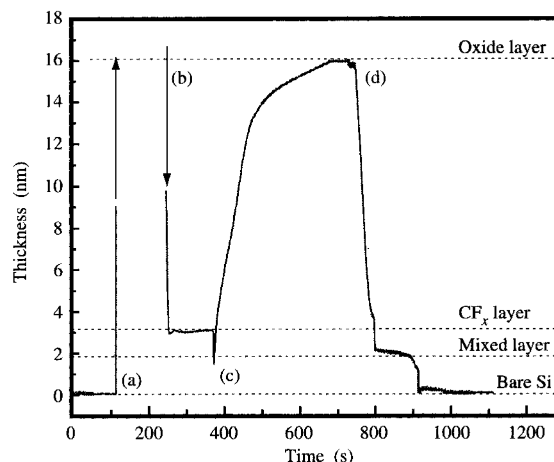

Figure 14

Time evolution of the thickness of different dielectric layers on silicon that are formed during fluorocarbon-based etching and subsequent surface cleaning [50]. At (a), the clean Si surface was exposed to a CHF_3 plasma and a thick fluorocarbon layer formed on the surface; at (b), a bias was applied to the sample and the film was etched away to its steady-state thickness; at (c), an O_2 plasma was ignited, and a portion of the fluorocarbon layer was removed before a thick oxide began to grow; finally, at (d), Ar^+ sputtering returned the surface to a clean state.

The results reported for Si extend quite well for copper, producing a clean Cu surface after the final Ar plasma process. An interesting response of the Cu to the fluorocarbon plasma exposure is the absence of the reacted layer seen with many other materials [50]. This is illustrated by the XPS spectra in **Figure 16**. Although the intensity seen in part (b) was much less than after the Ar plasma step, the ratio of reacted to unreacted Cu was extremely small in both cases. Only after the O_2 plasma cleaning step was a significant amount of reacted copper observed.

The demonstration of *in situ* HDP cleaning processes for blanket substrates must be extended to high-aspect-ratio structures. Both via bottom and sidewall issues must be addressed; e.g., the sidewall films (veils) must be removed [50]. The stability of novel organic dielectric materials when exposed to cleaning is also a critical issue and has been addressed in other work [50].

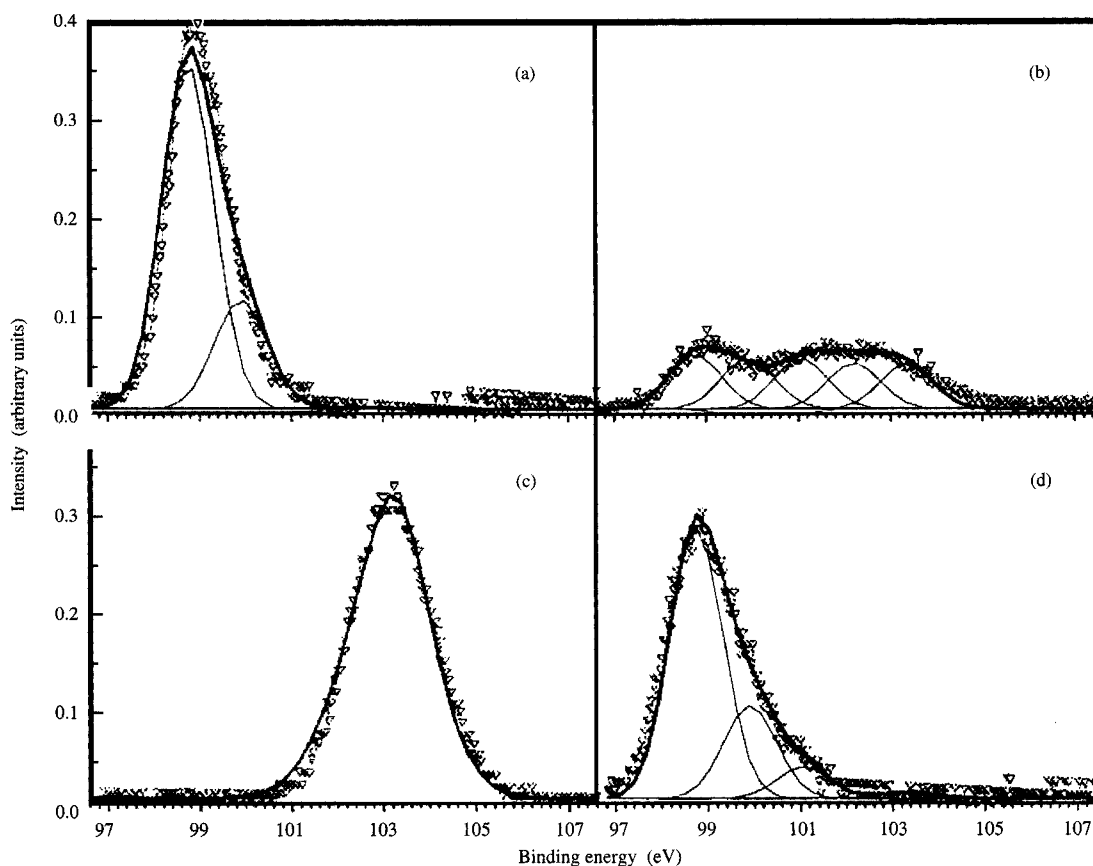

Figure 15

Silicon 2p XPS spectra for Si at a grazing electron emission angle for (a) an HF-dipped reference sample; (b) after exposure to a CHF_3 discharge; (c) after an O_2 plasma-cleaning step; and (d) after the final Ar^+ sputtering treatments of Figure 14. From [50], with permission.

Selective removal of Si_3N_4 stopping layer For the self-aligned contact-etching process, the Si_3N_4 etch-stop layer must be removed after SiO_2 etching and resist-stripping processes, with a high selectivity relative to SiO_2 and Si. This can be achieved by remote plasma-based removal of the Si_3N_4. The following steps are required: First, breaking through the oxynitride layer (formed by oxidation of the nitride during the resist and fluorocarbon removal process in O_2; see above). For this purpose, NF_3 is commonly used, since it minimizes the selectivity of Si_3N_4-to-SiO_2 etching. Second, the bulk Si_3N_4 film must be removed with a high selectivity with respect to SiO_2. A $CF_4/O_2/N_2$ system is sometimes used for this part of the process [51]. The study of this etching system in a downstream reactor illustrates the surface chemical interactions that can occur when reactive radicals formed in the gas phase dominate the etching kinetics by reducing reaction barriers. The sensitivity of the etching reaction in a downstream etching reactor to small changes in gas composition is due to the absence of ion bombardment at the etching surface.

Figure 17 shows the etching rates (ERs) of Si_3N_4 in $CF_4/O_2/N_2$ as a function of added O_2 and N_2 using a 400-W microwave discharge operated at a pressure of 0.5 Torr and a constant flow of CF_4. For CF_4/O_2 mixtures without N_2, the Si_3N_4 etching rate changes very little upon injection of O_2 to CF_4, despite the well-known increase of the F atom concentration by nearly a factor of 10 due to oxidation of fluorocarbon radicals [30, 31]. This behavior indicates that the Si_3N_4 etching rate cannot be limited by the arrival of fluorine atoms on the Si_3N_4 surface. Significant enhancements of the Si_3N_4 etching rate were observed upon injection of 5% N_2 (by a factor of 7× for an O_2/CF_4 ratio of 0.15). At the same time, the SiO_2 etching rate changed very little, enabling highly selective

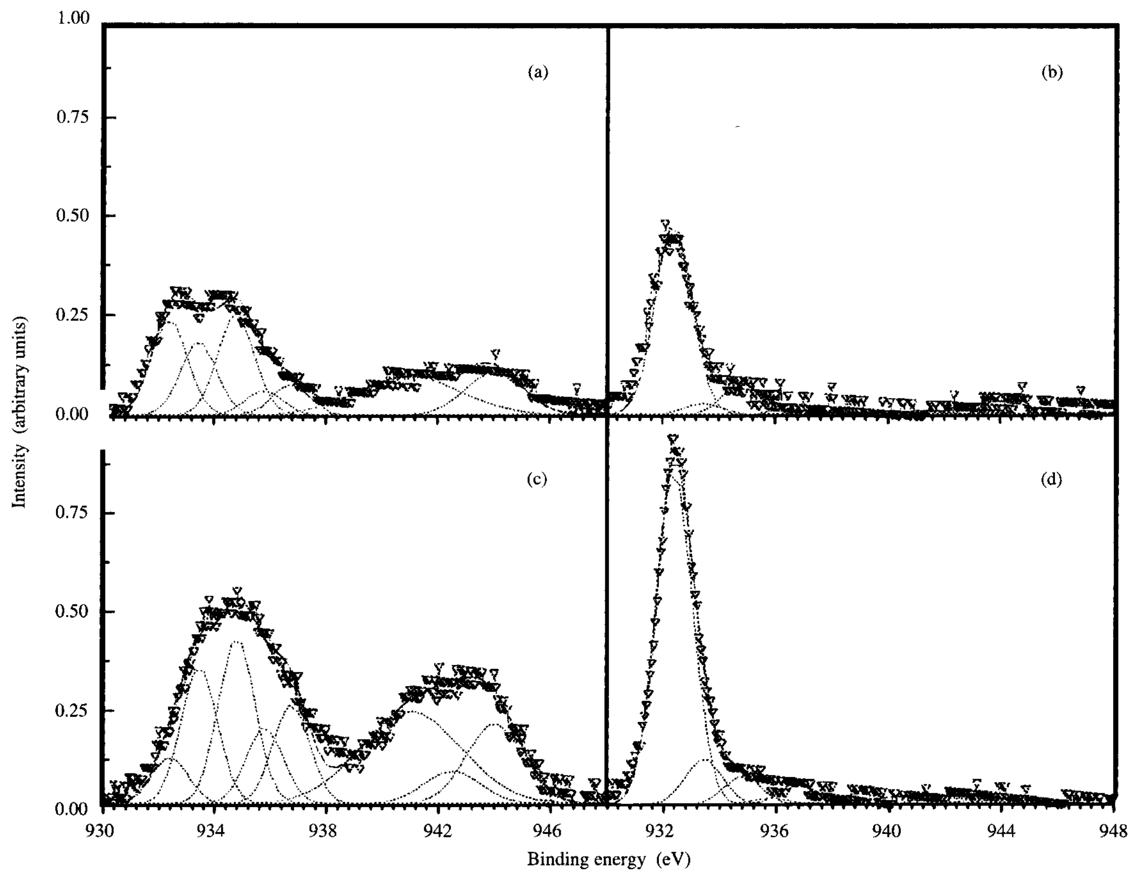

Figure 16

Copper 2p XPS spectra for Cu at a grazing electron emission angle for (a) an as-received Cu surface; (b) after fluorocarbon plasma exposure; (c) after an O_2 plasma-cleaning step; and (d) after a final Ar^+ sputtering step. Note that the intensity in (d) has been divided by four. From [50], with permission.

etching of Si_3N_4 over SiO_2 using $CF_4/O_2/N_2$. An examination of the fluorine density in the discharge region and in the downstream chamber showed that N_2 injection did not increase the F-atom concentration. A survey of various nitrogen-related species by mass spectrometry resulted in the conclusion that the NO mass spectrometric signal correlated best with the Si_3N_4 etching rate (see Figure 17). The production of a large concentration of free fluorine is necessary for significant Si_3N_4 etching, but it is not a sufficient condition, e.g., as is the case for a silicon thin film. This can be explained by the fact that Si_3N_4 is thermodynamically more stable than Si. For Si_3N_4, the breaking of the SiN bond is one important barrier in the overall etching reaction. A surface reaction model in which NO attacks a Si–N bond at the Si_3N_4 surface, producing N_2, which desorbs and leaves a Si–O species on the surface, has been proposed [29] and is supported by the gas-phase and surface characterization data shown in **Figures 18** and **19** [53].

The key role of NO in the etching of Si_3N_4 has been verified directly in experiments in which NO was injected downstream from a fluorine-based discharge, as first performed by Blain et al. [54]. The Si_3N_4 etching rate increased almost linearly with the flow of NO injected downstream. In Figure 18, data for Si_3N_4 surfaces etched in CF_4/O_2 (400/20 sccm) with either NO or no NO injected downstream are compared. Consistent with the surface reaction model outlined above [29], injection of NO leads to an enhancement of the Si_3N_4 etching rate by a factor of roughly 8, while concurrently oxidizing the Si_3N_4 surface. The indicated peak (oxygen 1s peak) has been attributed to SiO bonding.

Additional mass-spectrometry work shown in Figure 19 has provided additional support for this model. Intensity

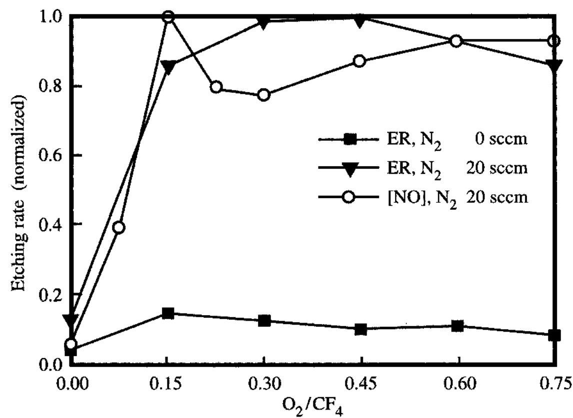

Figure 17

Etching rates of Si_3N_4 in a $CF_4/O_2/N_2$ plasma as a function of O_2 flow in the CF_4, as determined from mass-spectrometry intensities. The data were obtained using a microwave plasma-etching system, with the unbiased wafer located downstream from the plasma. Data for NO obtained under the same conditions are also shown. From [29], with permission.

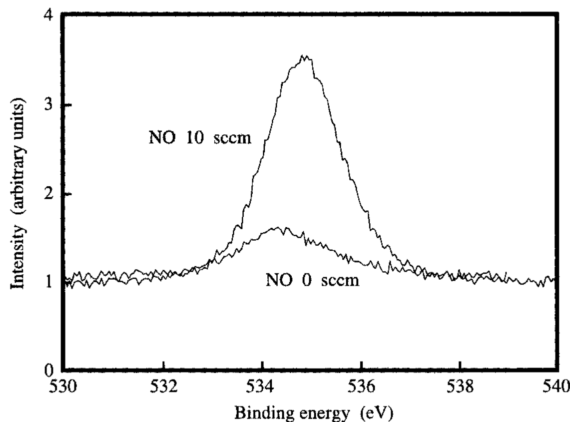

Figure 18

Mass-spectrometry intensities, indicating evidence of increased oxidation of a Si_3N_4 surface upon injection of NO downstream from a CF_4/O_2 discharge. The Si_3N_4 etching rate increased by a factor of 8 as a result of the NO injection. From [52], with permission.

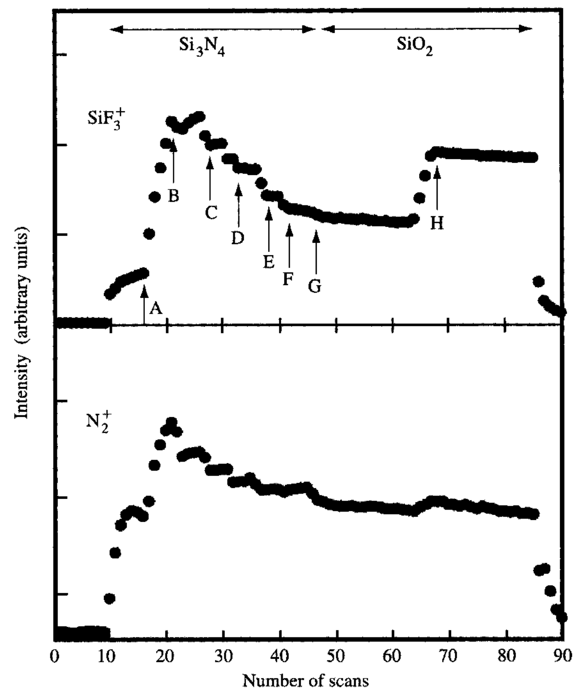

Figure 19

Mass-spectrometry intensities for SiF_3^+ and N_2^+ during the etching of Si_3N_4 and SiO_2 in a SF_6/NO 300/50-sccm discharge operated at 500 mTorr and 700 W microwave power. At point A, NO gas was injected downstream into the reactor, increasing the Si_3N_4 etching rate and increasing the SiF_3^+ and N_2^+ signals in the mass spectrometer. At points B, C, D, E, and F, the distance between the sample and the mass-spectrometer orifice was increased from 0.7 cm to 4 cm. The decrease of the SiF_3^+ and N_2^+ signals indicated that both products are produced by the etching of the Si_3N_4. At point G the Si_3N_4 film had been completely removed (as shown by ellipsometry), and etching of the SiO_2 began. At point H the distance between the sample and the mass-spectrometer orifice was again reduced to 0.7 cm, leading to an increase in the SiF_3^+ signal. From [52], with permission.

changes of the etch-product signals were determined for different processing conditions. A SF_6/O_2 mixture was used to etch a thin-film stack consisting of $Si_3N_4/SiO_2/Si$. SF_6 was chosen as a fluorine source to avoid the mass interference due to CO at mass 28. Figure 19 shows SiF_4 (SiF_3^+) and N_2 (N_2^+) product signals from Si_3N_4 etching as a function of time. At point A, NO gas was injected at a flow rate of 20 sccm downstream into the reactor, increasing the Si_3N_4 etching rate. This was mirrored in the growth of the SiF_3^+ signal by roughly a factor of 8. In addition, the N_2^+ signals increased. At points B, C, D, E, and F, the sample–mass-spectrometer-orifice distance was increased in steps from 0.7 cm to 4 cm, to ascertain whether the SiF_3^+ and N_2^+ signals were produced at the Si_3N_4 surface. A consistent decrease of the SiF_3^+ and N_2^+ signals showed that both products were produced by the etching of the Si_3N_4. At point G, the Si_3N_4 film had been completely removed (as shown by simultaneous ellipsometry), and etching of the SiO_2 began. At point H,

the distance between the sample and the mass-spectrometer orifice was again reduced to 0.7 cm, leading to an increase of the SiF_3^+ signal. These experiments showed that next to SiF_4, N_2 is an important second etching product. N_2O^+, NF_2^+, and N^+ signals were also monitored during the same experiment. These measurements showed that N_2O and NF_3 are also produced by the etching of Si_3N_4, but they vary much less significantly upon NO injection than does the N_2 signal.

- *Fundamental data on plasma–surface interactions by controlled-beam studies*

The example discussed in the preceding section illustrates the complexity of the surface processes that must be understood and controlled in microstructure fabrication. It is clear that even if one could characterize in complete detail the incident fluxes, surface processes, and outgoing fluxes, it would be very difficult to mechanistically isolate the effects of the various incident particle fluxes applicable to an actual plasma environment. This is due to the significant interactions between different particle fluxes on surfaces, which make it difficult to establish cause and effect. Several investigators have therefore attempted to "simulate" the plasma–surface interaction in a UHV apparatus using beams of different plasma species at relevant energies, e.g., ions and neutrals [25]. Using this approach, Coburn and Winters [55] have demonstrated how ion bombardment can enhance an etching reaction and that synergistic effects between ions and neutrals that strike the surface simultaneously can be very large for certain systems, e.g., the fluorine–silicon–Ar^+ system [25, 55]. They have attributed their results to chemical sputtering. In general, neutral/ion/surface interactions give rise to complex processes, with the outcome depending critically on the energy content of the neutrals, the substrate surface temperature [56, 57] and the ion/neutral reactant flux ratio [58–60].

The reactive beam approach appears to be useful for obtaining a database for the interaction of reactive plasma particles with surfaces of electronic materials [61]. A first requirement is that sources be available that can produce well-characterized, clean beams of realistic ions and realistic neutrals at all energies of interest. It is essential that realistic ions be used in the beam experiments [62], since the ions are often not just an energy carrier, but (especially in high-density plasma systems) also carry a significant fraction of the reactive species to the surface. The interaction of these particle beams with pristine and realistic surfaces must be studied to determine reaction probabilities and rates, reaction products and their energy content, the importance of interactive effects for multiple beams, and the nature of the steady-state surface reaction layer. These data are a prerequisite for realistic computer modeling of the plasma–surface interactions that are crucial in comprehensive computer modeling of plasma-etching processes.

Conclusions

For planar surfaces, impressive experimental techniques exist that can be used to obtain the information required to develop a quantitative description of plasma–surface interactions relevant to plasma etching. A strong need exists to develop and employ beam sources of realistic plasma species in order to facilitate controlled investigations of relevant plasma–surface interactions. An improved understanding of the interaction of specific reactive particles with a surface and the synergistic effects that become important when several species react simultaneously, coupled with modeling, should make it possible to identify key mechanisms. The situation is not as promising for microstructures. Novel phenomena that are absent for surfaces occur in microstructures and ultimately determine the usefulness of a particular plasma process. Significant efforts will be needed to further develop means to establish particle fluxes and identify fundamental surface processes in microstructures as a function of microstructural dimensions.

Acknowledgments

The experimental work described in this paper was supported by SEMATECH, Sandia National Laboratories, Lam Research, Air Products, Leybold Inficon, the Semiconductor Research Corporation, the New York State Science and Technology Foundation, and the Department of Energy under Contract No. DE-FG02-97ER54445. We also acknowledge helpful discussions and collaboration with M. Blain, H.-O. Blom, M. Chang, J. M. Cook, Th. Dao, K. Donohoe, R. Ellefson, L. Frees, Ch. Hedlund, J. Langan, G. Powell, and P. Ryan.

References

1. G. S. Oehrlein and J. F. Rembetski, *IBM J. Res. Develop.* **36,** 140 (1992).
2. G. S. Oehrlein, *Surf. Sci.* **386,** 222 (1997).
3. M. A. Lieberman and A. J. Lichtenberg, *Principles of Plasma Discharges and Materials Processing*, John Wiley & Sons, Inc., New York, 1994.
4. K. Nojiri, E. Iguchi, K. Kawamura, and K. Kadota, Bus. Center Acad. Soc. Jpn., Tokyo, 1989, p. 153.
5. R. A. Gottscho, C. W. Jurgensen, and D. J. Vitkavage, *J. Vac. Sci. Technol. B* **10,** 2133 (1992).
6. I. P. Herman, *Optical Diagnostics for Thin Film Processing*, Academic Press, Inc., New York, 1996.
7. H. Sugai, H. Kojima, A. Ishida, and H. Toyoda, *Appl. Phys. Lett.* **56,** 2616 (1990).
8. Y. Hikosaka, M. Nakamura, and H. Sugai, *Jpn. J. Appl. Phys.* **33,** 2157 (1994).
9. E. R. Fisher, P. Ho, W. G. Breiland, and R. J. Buss, *J. Phys. Chem.* **96,** 9855 (1992).
10. G. S. Oehrlein, *J. Vac. Sci. Technol. A* **11,** 34 (1993).
11. E. S. Aydil, R. A. Gottscho, and Y. J. Chabal, *Pure & Appl. Chem.* **66,** 1381 (1994).

12. E. S. Aydil and R. A. Gottscho, *Semicond. Sci. Technol.* **40,** 181 (1997).
13. J. C. Arnold and H. H. Sawin, *J. Appl. Phys.* **70,** 5314 (1991).
14. M. Schaepkens and G. S. Oehrlein, *Appl. Phys. Lett.* **72,** 1293 (1998).
15. K. Kurihara and M. Sekine, *Plasma Sources Sci. Technol.* **5,** 121 (1996).
16. O. Joubert, G. S. Oehrlein, and Y. Zhang, *J. Vac. Sci. Technol. A* **12,** 658 (1994).
17. O. Joubert, G. S. Oehrlein, M. Surendra, and D. Zhang, *J. Vac. Sci. Technol. A* **12,** 1957 (1994).
18. G. S. Oehrlein, K. K. Chan, M. A. Jaso, and G. W. Rubloff, *J. Vac. Sci. Technol. A* **7,** 1030 (1989).
19. G. S. Oehrlein, J. F. Rembetski, and E. H. Payne, *J. Vac. Sci. Technol. B* **8,** 1199 (1990).
20. M. Haverlag, G. S. Oehrlein, and D. Vender, *J. Vac. Sci. Technol. B* **12,** 96 (1994).
21. K. V. Guinn and V. M. Donnelly, *J. Appl. Phys.* **75,** 2227 (1994).
22. K. V. Guinn, C. C. Cheng, and V. M. Donnelly, *J. Vac. Sci. Technol. B* **13,** 214 (1995).
23. F. H. Bell, O. Joubert, and L. Vallier, *J. Vac. Sci. Technol. B* **14,** 1796 (1996).
24. O. Joubert, P. Czuprynski, F. H. Bell, P. Berruyer, and R. Blanc, *J. Vac. Sci. Technol. B* **15,** 629 (1997).
25. H. F. Winters and J. W. Coburn, *Surf. Sci. Rep.* **14,** 161 (1992).
26. J. Givens, S. Geissler, J. Lee, O. Cain, J. Marks, P. Keswick, and C. Cunningham, *J. Vac. Sci. Technol. B* **12,** 427 (1994).
27. M. Schaepkens, G. S. Oehrlein, C. Hedlund, L. B. Jonsson, and H.-O. Blom, *J. Vac. Sci. Technol. A* **16,** 3281 (1998).
28. N. R. Rueger, J. J. Beulens, M. Schaepkens, M. F. Doemling, J. M. Mirza, T. E. F. M. Standaert, and G. S. Oehrlein, *J. Vac. Sci. Technol. A* **15,** 1881 (1997).
29. B. E. E. Kastenmeier, P. J. Matsuo, J. J. Beulens, and G. S. Oehrlein, *J. Vac. Sci. Technol. A* **14,** 2802 (1996).
30. P. J. Matsuo, B. E. E. Kastenmeier, J. J. Beulens, and G. S. Oehrlein, *J. Vac. Sci. Technol. A* **15,** 1801 (1997).
31. *Plasma Etching*, D. M. Manos and D. L. Flamm, Eds., Academic Press, Inc., San Diego, 1989.
32. J. P. Simko and G. S. Oehrlein, *J. Electrochem. Soc.* **138,** 2748 (1991).
33. J. W. Butterbaugh, D. C. Gray, and H. H. Sawin, *J. Vac. Sci. Technol. B* **9,** 1461 (1991).
34. R. A. Heinecke, *Solid State Electron.* **18,** 1146 (1975).
35. L. M. Ephrath and E. J. Petrillo, *J. Electrochem. Soc.* **129,** 2282 (1982).
36. M. Schaepkens, T. E. F. M. Standaert, P. G. M. Sebel, G. S. Oehrlein, and J. M. Cook, *J. Vac. Sci. Technol. A* **17,** 1 (1999).
37. E. M. van Veldhuizen, T. Bisschops, E. J. W. van Vliembergen, and J. H. M. C. van Wolfput, *J. Vac. Sci. Technol. A* **3,** 2205 (1985).
38. T. E. F. M. Standaert, M. Schaepkens, P. G. M. Sebel, N. R. Rueger, and G. S. Oehrlein, *J. Vac. Sci. Technol. A* **16,** 239 (1998).
39. G. S. Oehrlein, C. M. Ransom, S. N. Chakravarti, and Y. H. Lee, *Appl. Phys. Lett.* **46,** 686 (1985).
40. G. S. Oehrlein and H. L. Williams, *J. Appl. Phys.* **62,** 662 (1987).
41. C. Hedlund, C. Strandman, I. V. Katardjiev, Y. Bäcklund, S. Berg, and H.-O. Blom, *J. Vac. Sci. Technol. B* **14,** 3239 (1996).
42. R. Behrisch, *Sputtering by Particle Bombardment I*, Springer Verlag, Heidelberg, 1981.
43. R. Behrisch, *Sputtering by Particle Bombardment II*, Springer Verlag, Heidelberg, 1983.
44. R. Behrisch and K. Wittmaack, *Sputtering by Particle Bombardment III*, Springer Verlag, Heidelberg, 1991.
45. G. S. Oehrlein, D. Zhang, D. Vender, and M. Haverlag, *J. Vac. Sci. Technol. A* **12,** 323 (1994).
46. G. S. Oehrlein, D. Zhang, D. Vender, and O. Joubert, *J. Vac. Sci. Technol. A* **12,** 333 (1994).
47. D. J. Economou and R. C. Alkire, *J. Electrochem. Soc.* **135,** 941 (1988).
48. S. G. Ingram, *J. Appl. Phys.* **68,** 500-4 (1990).
49. M. F. Doemling, N. R. Rueger, G. S. Oehrlein, and J. M. Cook, *J. Vac. Sci. Technol. B* **16,** 1998 (1998).
50. P. J. Matsuo, S. Allen, T. E. F. M. Standaert, G. S. Oehrlein, and T. Dalton, *J. Vac. Sci. Technol. A* **17** (1999), in press.
51. *Applications of Plasma Processes to VLSI Technology*, T. Sugano, Ed., John Wiley & Sons, Inc., New York, 1985.
52. B. E. E. Kastenmeier, P. J. Matsuo, G. S. Oehrlein, and J. G. Langan, *J. Vac. Sci. Technol. A* **16,** 2047 (1998).
53. B. E. E. Kastenmeier, P. J. Matsuo, G. S. Oehrlein, R. Ellefson, and L. Frees, *J. Vac. Sci. Technol. A* **17** (1999) in press.
54. M. G. Blain, T. L. Meisenheimer, and J. E. Stevens, *J. Vac. Sci. Technol. A* **14,** 2151 (1996).
55. J. W. Coburn and H. F. Winters, *J. Appl. Phys.* **50,** 3189 (1979).
56. L. A. DeLouise, *J. Chem. Phys.* **94,** 1528 (1991).
57. L. A. DeLouise, *J. Vac. Sci. Technol. A* **9,** 1732 (1991).
58. L. A. DeLouise, *J. Appl. Phys.* **70,** 1718 (1991).
59. D. C. Gray, I. Tepermeister, and H. H. Sawin, *J. Vac. Sci. Technol. B* **11,** 1243 (1993).
60. J. P. Chang, J. C. Arnold, G. C. H. Zau, Hyung-Shik Shin, and H. H. Sawin, *J. Vac. Technol. A* **15,** 1853 (1997).
61. D. B. Graves, M. J. Kushner, J. W. Gallagher, A. Garscadden, G. S. Oehrlein, and A. V. Phelps, *Database Needs for Modeling and Simulation of Plasma Processing,* National Research Council, Panel on Database Needs in Plasma Processing, National Academy Press, Washington, DC, 1996.
62. W. H. Chang, I. Bello, and W. M. Lau, *J. Vac. Sci. Technol. A* **11,** 1221 (1993).
63. H. F. Winters and J. W. Coburn, *Mater. Res. Soc. Symp. Proc.* **38,** 189 (1985).
64. H. F. Winters, in *Plasma Chemistry III*, S. Veprek and M. Venugopalan, Eds., Springer Verlag, Heidelberg, 1980, p. 69.
65. T. J. Chuang, H. F. Winters, and J. W. Coburn, *Appl. Surf. Sci.* **2,** 514 (1978).
66. H. F. Winters, H. Coufal, C. T. Rettner, and D. S. Bethune, *Phys. Rev. B* **41,** 6240 (1990).
67. G. S. Oehrlein and G. J. Scilla, *Radiation Effects in Defects & Solids* **111+112,** 299 (1989).
68. G. S. Oehrlein, R. G. Schad, and M. A. Jaso, *Surf. Interface Anal.* **8,** 243 (1986).
69. Y. Horiike, in *VLSI Electronics Microstructure Science, Volume 8, Plasma Processing for VLSI*, N. G. Einspruch and D. M. Brown, Eds., Academic Press, Inc., New York, 1984, p. 448.
70. M. Sekine, H. Okano, K. Yamabe, N. Hayasaka, and Y. Horiike, Bus. Center Acad. Soc. Jpn., Tokyo, 1985, p. 82.
71. A. J. Yencha, in *Electron Spectroscopy,* Vol. 5, Academic Press, London, 1984, p. 197.

Received February 20, 1998; accepted for publication August 3, 1998

Gottlieb S. Oehrlein *University at Albany, State University of New York, Albany, New York 12222.* Professor Oehrlein received a Ph.D. in physics from the University at Albany in 1981. From 1982 to 1993 he was a Research Staff Member at the IBM Thomas J. Watson Research Center in Yorktown Heights, New York. In September 1993 he joined the faculty of the Department of Physics at the State University of New York (SUNY) at Albany. Professor Oehrlein has published more than 150 papers and contributed significant results on the use of low-temperature plasmas for materials processing. These contributions were recognized with several awards at the IBM Research Division, the 1992 Electronics Division Award of the Electrochemical Society, and, in 1993, the 14th Thinker Award of the Tegal Corporation.

Marcus F. Doemling *University at Albany, State University of New York, Albany, New York 12222.* Mr. Doemling is working toward his Ph.D. in the Plasma Research Laboratory at SUNY Albany. He received a Vordiplom degree in physics from Würzburg University in Germany, and in 1995 an M.S. degree in physics from SUNY at Albany. He has worked on high-density plasma etching of materials, especially photoresist. His research is currently focused on reactive ion beam etching (RIBE) to establish fundamental process parameters applicable to plasma-based etching processes.

Bernd E. E. Kastenmeier *University at Albany, State University of New York, Albany, New York 12222.* Mr. Kastenmeier began his study of physics at the University at Würzburg, Germany, in 1990. In 1993, after receiving a Vordiplom degree, he began graduate studies in the Physics Department of SUNY at Albany. He received an M.S. degree in physics from SUNY in 1994 and is currently working toward his Ph.D. degree. Mr. Kastenmeier's research activities are centered around the processing of materials using remote plasmas. He has studied the etching mechanism of materials used in integrated-circuit manufacturing in reactive afterglows of microwave discharges, employing surface analytical methods and mass spectrometry. He has also improved the selective stripping of silicon nitride and has investigated the efficiency of different F-containing gases for the cleaning of deposition reactors.

Peter J. Matsuo *University at Albany, State University of New York, Albany, New York 12222.* Mr. Matsuo received a B.S. in physics and mathematics in 1994 and an M.S. in physics from SUNY at Albany in 1995, after which he joined the Plasma Research Laboratory at SUNY Albany for his doctoral studies. His research has focused on the plasma cleaning of dielectrics and metallization layers. He is currently the author of five published articles and one patent.

Neal R. Rueger *University at Albany, State University of New York, Albany, New York 12222.* Mr. Rueger has been working at the Plasma Research Laboratory at SUNY at Albany since it was established in late 1993. He received a B.S. from SUNY at Binghamton in 1983, with a major in geophysics. He received an M.S. in physics from SUNY at Albany in 1992, and is currently completing his Ph.D. His areas of research are high-density plasma etching of silicon dioxide, silicon, and photoresist employing inductively coupled plasmas, as well as reactive ion beam etching studies focused on the establishment of the fundamental details of the plasma-etching process.

Marc Schaepkens *University at Albany, State University of New York, Albany, New York 12222.* Mr. Schaepkens is working toward his Ph.D. degree in physics in the Plasma Research Laboratory of SUNY at Albany. He received an Ingenieur Diploma/M.S. in applied physics from the Eindhoven University of Technology, Netherlands, in 1996, and an M.S. in physics from SUNY Albany in 1997. His primary research projects are the study of the mechanisms underlying selective SiO_2 etching and the etching of high-aspect-ratio features using inductively coupled fluorocarbon plasmas.

Theodorus E. F. M. Standaert *University at Albany, State University of New York, Albany, New York 12222.* In 1995 Mr. Standaert joined the Plasma Research Laboratory at SUNY at Albany, where he has been studying the competitive process between fluorocarbon deposition and etching in high-density plasmas. This study completed a four-year education in applied physics, for which he received an Ingenieur (Ir.) degree in 1996 from the Eindhoven University of Technology, Netherlands. As part of his doctoral research, he has been working on the patterning of novel low-K dielectrics and ultranarrow (~20-nm) trenches using high-density plasmas.